Research Article

Maraviroc promotes recovery from traumatic brain injury in mice by suppression of neuroinflammation and activation of neurotoxic reactive astrocytes

Xi-Lei Liu[1, 2, 3, #], Dong-Dong Sun[4, #], Mu-Tian Zheng[1, 2, 3, #], Xiao-Tian Li[1, 2, 3], Han-Hong Niu[3, 5], Lan Zhang[3, 6, 7], Zi-Wei Zhou[1, 2], Hong-Tao Rong[1, 2], Yi Wang[1, 2], Ji-Wei Wang[4], Gui-Li Yang[2], Xiao Liu[2], Fang-Lian Chen[2], Yuan Zhou[1, 2, *], Shu Zhang[2, *], Jian-Ning Zhang[1, 2, 3, *]

From the Contents

Graphical Abstract

Maraviroc improves recovery of neurological function in mice after traumatic brain injury by inhibiting the activation of neuroinflammation and neurotoxic reactive astrocytes
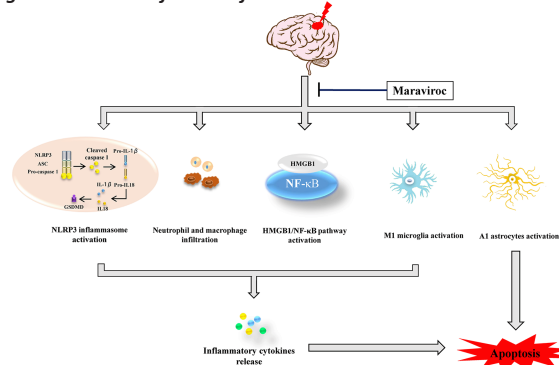
Abstract

Neuroinflammation and the NACHT, LRR, and PYD domains-containing protein 3 inflammasome play crucial roles in secondary tissue damage following an initial insult in patients with traumatic brain injury (TBI). Maraviroc, a C-C chemokine receptor type 5 antagonist, has been viewed as a new therapeutic strategy for many neuroinflammatory diseases. We studied the effect of maraviroc on TBI-induced neuroinflammation. A moderate-TBI mouse model was subjected to a controlled cortical impact device. Maraviroc or vehicle was injected intraperitoneally 1 hour after TBI and then once per day for 3 consecutive days. Western blot, immunohistochemistry, and TUNEL (terminal deoxynucleotidyl transferase-mediated dUTP nick-end labeling) analyses were performed to evaluate the molecular mechanisms of maraviroc at 3 days post-TBI. Our results suggest that maraviroc administration reduced NACHT, LRR, and PYD domains-containing protein 3 inflammasome activation, modulated microglial polarization from M1 to M2, decreased neutrophil and macrophage infiltration, and inhibited the release of inflammatory factors after TBI. Moreover, maraviroc treatment decreased the activation of neurotoxic reactive astrocytes, which, in turn, exacerbated neuronal cell death. Additionally, we confirmed the neuroprotective effect of maraviroc using the modified neurological severity score, rotarod test, Morris water maze test, and lesion volume measurements. In summary, our findings indicate that maraviroc might be a desirable pharmacotherapeutic strategy for TBI, and C-C chemokine receptor type 5 might be a promising pharmacotherapeutic target to improve recovery after TBI.

Key Words: C-C chemokine receptor type 5 (CCR5) antagonist; high mobility group protein B1 (HMGB1); maraviroc; M1 microglia; nuclear factor-κB pathway; NACHT, LRR, and PYD domains-containing protein 3 (NLRP3) inflammasome; neuroinflammation; neurological function; neurotoxic reactive astrocytes; traumatic brain injury

Introduction

Traumatic brain injury (TBI) can result in neurological disorders or death and remains a heavy burden to families and society worldwide. However, there are currently no effective treatment guidelines to mitigate the brain damage caused by TBI (Maas et al., 2017). The primary injury occurs immediately after the initial insult and can lead to cerebral contusion, cranial hematoma, and axonal injury. A variety of secondary events follow the initial insult and comprise oxidative stress, blood-brain barrier (BBB) disruption, neuroinflammation, and apoptosis (Corps et al., 2015; Johnson et al., 2018; Ismail et al., 2020). The pathogenesis of TBI is regulated by the immune system and neuroinflammation, including innate and adaptive immunity, resident microglial activation, cytokine release, and inflammasome activation (Jassam et al., 2017).

Microglia and peripheral immunocytes move to the core of the initial insult to defend against pathogens and therefore contribute to secondary injury after TBI (Corps et al., 2015). Microglia polarize into two phenotypes: classically activated M1 microglia and alternatively activated M2 microglia (Jassam et al., 2017; Simon et al., 2017). The M1 phenotype releases proinflammatory mediators that aggravate brain tissue damage. In contrast, alternatively activated M2 microglia aid brain recovery by secreting anti-inflammatory factors (Wang et al., 2013; Hu et al., 2015). In addition, it is well established that nucleotide-binding oligomerization domain-like receptor family activation

[1]Department of Neurosurgery, Tianjin Medical University General Hospital, Tianjin, China; [2]Tianjin Neurological Institute, Key Laboratory of Post-Neuroinjury Repair and Regeneration in Central Nervous System, Tianjin, China; [3]Graduate School, Tianjin Medical University, Tianjin, China; [4]Department of Neurosurgery, Tianjin Huanhu Hospital, Tianjin Key Laboratory of Cerebral Vascular and Neurodegenerative Diseases, Tianjin Neurosurgical Institute, Tianjin, China; [5]Department of Radiotherapy, Tianjin Medical University General Hospital, Tianjin, China; [6]Department of Geriatrics, Tianjin Medical University General Hospital, Tianjin, China; [7]Institute of Tianjin Geriatrics, Tianjin Medical University General Hospital, Tianjin, China
*Correspondence to: Yuan Zhou, PhD, zy963000@126.com; Shu Zhang, PhD, gloria523@163.com; Jian-Ning Zhang, PhD, jianningzhang@hotmail.com.
https://orcid.org/0000-0002-4055-9947 (Yuan Zhou); https://orcid.org/0000-0003-3627-863X (Shu Zhang); https://orcid.org/0000-0002-7290-0994 (Jian-Ning Zhang)
#These authors contributed equally to this study.

is a trigger of cell pyroptosis and leads to poor outcomes after brain injury (O'Brien et al., 2020). NACHT, LRR, and PYD domains-containing protein 3 (NLRP3) has been studied in a number of acute central nervous system (CNS) disorders (Ren et al., 2018; Xu et al., 2018a; Sun et al., 2019; Chen et al., 2020). The NLRP3 inflammasome consists of the sensor protein NLRP3, the apoptosis-associated speck-like protein adapter, and the precursor enzyme pro-caspase-1. Interleukin (IL)-1β, IL-18, and the amino terminus of gasdermin-D are cleaved by activated caspase-1 from inactive proisomers to their active forms. These proteins ultimately lead to cell disruption accompanied by rapid secretion of proinflammatory cytokines (Franke et al., 2021). Thus, reduction of activation of the NLRP3 inflammasome and M1 microglia might be a promising therapeutic strategy for TBI.

Recent studies reported that CNS injury and disease could stimulate polarization of astrocytes into two different phenotypes, termed neurotoxic A1 reactive astrocytes and neuroprotective A2 reactive astrocytes, which express complement C3 and protein S100-A10, respectively (Diaz-Castro et al., 2019; Miyamoto et al., 2020; Peng et al., 2020). The astroglial transition from a resting state to the neurotoxic A1 reactive astrocyte state is activated by IL-1α, tumor necrosis factor (TNF), and complement C1q, which are released by microglia and cause the death of neuronal cells. A2 astrocytes are activated by ischemia-hypoxia and may play a neuroprotective role in CNS diseases (Liddelow et al., 2017). A1 astrocytes that highly express complement C3 were able to kill neurons and oligodendrocytes in CNS diseases by releasing very-long-chain fatty acid acyl chains and free fatty acids (Escartin et al., 2021). However, the A1 and A2 astrocyte polarization theories remain controversial. The authors of a review of reactive astrocytes argued that it is not appropriate to simply divide reactive astrocytes into A1 and A2 phenotypes and suggested that astrocytes in CNS diseases should be termed 'reactive astrocytes' (Escartin et al., 2021). Although nomenclature and definitions of reactive astrocytes need to be clarified, inhibiting the activation of neurotoxic astrocytes is important to the survival of neurons.

Maraviroc was the first C-C chemokine receptor type 5 (CCR5) antagonist licensed by the U.S. Food and Drug Administration and has been viewed as a new therapeutic strategy to treat neuroinflammatory diseases such as multiple sclerosis, Rasmussen encephalitis, and HIV-associated neurocognitive disorders (Martin-Blondel et al., 2016). According to recent studies, knockdown or pharmacological blocking of CCR5 enhanced motor function, strengthened learning and memory, decreased cognitive decline, and reduced lesion area and hippocampal neuron loss after stroke and TBI (Joy et al., 2019; Friedman-Levi et al., 2021). In addition, in vivo and in vitro experiments showed that CCR5 blockade decreases peripheral immune cell and microglia trafficking to the lesion region and exerts a protective effect by attenuating neuroinflammation (Glass et al., 2005; Rosi et al., 2005; Arberas et al., 2013). Taken together, these results suggested that CCR5 may be beneficial to patients suffering cerebral damage. Nevertheless, whether maraviroc alleviates TBI-induced microglial polarization and inflammasome activation has not been studied. Therefore, we hypothesized that maraviroc protects against TBI by suppressing NLRP3 inflammasome activation and modulating microglial and astrocyte polarization.

Methods

Animals

All experimental animal protocols were reviewed and approved by the Animal Care and Use Committee of Tianjin Medical University General Hospital, Tianjin, China, on January 20, 2020 (approval No. IRB2020-DW-19) and conducted in strict accordance with international laws and National Institutes of Health policies, including the Guide for the Care and Use of Laboratory Animals (8th ed., 2011). Male specific-pathogen-free C57BL/6J mice (8–10 weeks old, 22–25 g) used in the study were supplied by Beijing Vital River Laboratory Animal Technology Co., Ltd., Beijing, China (license No. SCXK (Jing) 2021-0006). The mice were housed in the animal facilities at 20 ± 2°C and 45% humidity under a 12-hour light/dark cycle with food and water ad libitum. All 60 mice were divided into three equal groups at random using the random number table method (n = 20/group): (1) sham group, (2) TBI + vehicle group, and (3) TBI + maraviroc group. The experimental results were obtained by a researcher who was blinded to the experimental states and treatment.

TBI model

A controlled cortical impact (CCI) device (eCCI-6.3 device, Custom Design & Fabrication, Inc., Sandston, VA, USA) was used on the mice to induce the experimental TBI model. Briefly, intraperitoneal injection of 1% sodium pentobarbital solution (6 mL/kg, Beijing Solarbio Science & Technology Co., Ltd., Beijing, China) was used to deeply anesthetize the mice. Then, the mice were placed in a stereotactic apparatus (RWD Life Science Co., Ltd., Shenzhen, China). Subsequently, a 3.0-mm-diameter hole was made centered between bregma and lambda and lateral to the sagittal suture on the right parietal bone. The skull cap was then removed gently to ensure that the dura was intact. The moderate TBI model was induced by CCI with the following parameters: depth of 1.8 mm, velocity of 4.5 m/s, and duration time of 200 ms. After TBI, the scalp was immediately closed with 6-0 silk sutures. Each mouse was placed on a heating pad to recover from the anesthesia, and then each mouse was housed in an individual cage. Mice in the sham group were anesthetized and had the skull cap removed without CCI.

Drug administration

Maraviroc (Selleck Chemicals LLC, Houston, TX, USA) was dissolved in 5% dimethyl sulfoxide, 40% polyethylene glycol 300, and 5% Tween 80 in saline, and 20 mg/kg maraviroc was injected intraperitoneally 1 hour after CCI and daily for the next 3 days. Mice receiving vehicle received identical proportions of dimethyl sulfoxide, polyethylene glycol 300, and Tween 80 in saline by intraperitoneal injection 1 hour after CCI or the sham operation. The dose of maraviroc (20 mg/kg) used in the study was selected in accordance with previous reports (Joy et al., 2019; Friedman-Levi et al., 2021).

Behavioral assessment
Modified neurological severity scores

Short-term neurological function was assessed by the modified neurological severity score (mNSS) as shown in **Additional Table 1**, which comprises tests to evaluate reflexes, alertness, coordination, and motor abilities. The mNSS was used to evaluate neurological function at 1, 3, 7, and 14 days post-TBI (n = 10/group). Lower scores imply better neurological outcomes.

Rotarod test

Motor coordination and balance were determined by the rotarod test (Sacks et al., 2018). The mice (n = 10/group) were placed on moving rotarod equipment (RWD Life Science Co., Ltd.) and tested using the rotarod protocol (Xu et al., 2018b). The mice received a trial at a slow speed (4 r/min) to familiarize them with the test and four consecutive trials with acceleration (from 4 to 40 r/min) to record baseline latency on the day before TBI. Data were collected at 1, 3, 7, and 14 days post-TBI. Each trial ended when the mouse fell off the rod or after a maximum of 5 minutes.

Morris water maze

The spatial learning and memory abilities of the mice were measured using a Morris water maze (MWM) 15–21 days post-TBI (Ran et al., 2020). The MWM pool consisted of a stainless steel cylindrical pool (122 cm in diameter and 51 cm in height) with a submerged hidden platform (10cm in diameter). The MWM apparatus was filled with water 22 ± 2°C and dyed white with nontoxic paint. The experiment was separated into two consecutive phases: a training phase of 15–20 days and a spatial memory test phase of 21 days. In the probe phase, there were 4 trials of the latency test each day, with 90 seconds for each test. The mice (n = 10/group) were placed in each quadrant of the pool in turn, from the first to the fourth quadrant. Then, they were allowed to seek the hidden platform for 90 seconds and to stay on the platform for 5 seconds. If a mouse did not find the platform within 90 seconds, it was placed on the platform for 15 seconds, and the time was recorded as 90 seconds. In the test phase, the mice were placed diagonally opposite the platform quadrant with the platform removed and allowed to find the platform site for 90 seconds. The platform crossing times, escape latency times, swimming traces, and the training phase were recorded and analyzed with a video tracking system (EthoVision XT 13, Noldus Information Technology, Wageningen, the Netherlands).

Western blotting

The mice (n = 5/group) were euthanized 3 days post-CCI. To prevent contamination of experimental results by blood proteins, the mice were transcardially perfused with cold phosphate-buffered saline (PBS). Brain samples were removed as previously reported (Chen et al., 2021) and homogenized with a triturator in ice-cold radioimmunoprecipitation assay buffer (Beijing Solarbio Science & Technology Co., Ltd.) with protease and phosphatase inhibitors (Beijing Solarbio Science & Technology Co., Ltd.) for 30 minutes. After centrifugation at 12,000 r/min at 4°C for 10 minutes, the supernatants of homogenates were collected, 4× loading buffer was added, and the samples were heated for 10 minutes at 95°C. Protein concentration was measured using a BCA (bicinchoninic acid) Protein Assay Kit (Thermo Fisher Scientific, Waltham, MA, USA). Equivalent protein (8 µg) was resolved using 10–15% sodium dodecyl sulfate-polyacrylamide gel electrophoresis gels. Then, the resolved proteins were transferred onto presoaked polyvinylidene fluoride membranes (MilliporeSigma, Burlington, MA, USA) by electroblotting, and the blots were incubated with 5% skim milk dissolved in Tris-buffered saline-Tween 20 at room temperature for 2 hours. Afterward, the membranes were incubated at 4°C for 24 hours with the primary antibodies shown in **Table 1**. The membranes were washed three times with Tris-buffered saline-Tween 20 buffer and subsequently submerged in the appropriate horseradish peroxidase-conjugated secondary antibody (1:5000, all from ZSGB-Bio, Beijing, China) at room temperature for 1 hour as follows: goat anti-rabbit (Cat# ZB-2301, RRID: AB_2747412), goat anti-mouse (Cat# ZB-2305, RRID: AB_2747415), goat anti-rat (Cat# ZB-2307), rabbit anti-goat (Cat# ZB-2306, RRID: AB_2868454). Protein bands were visualized with an enhanced chemiluminescence system (MilliporeSigma). The protein expression level was determined by ImageJ software (version 1.8.0, National Institutes of Health, Bethesda, MD, USA; Schneider et al., 2012) and was standardized to that of β-actin.

Immunohistochemical staining

At 3 days post-CCI, the mice (n = 5/group) were deeply anesthetized and killed by transcardiac perfusion with PBS followed by 4% paraformaldehyde. The brains were carefully removed and submerged overnight in 4% paraformaldehyde. The brains were moved to 15% and then 30% sucrose solutions over 24 hours at 4°C to dehydrate the tissue. After dehydration, the brains were cut into 5-mm sections as previously reported (Yan et al., 2020). The brain sections were immersed in optimal cutting compound temperature medium (Sakura Finetek USA, Torrance, CA, USA) and cut into 8-µm coronal sections using a cryostat microtome (CM1950, Leica Biosystems, Nußloch, Germany). The coronal sections were rinsed with PBS for 10 minutes to remove the optimal cutting compound temperature medium and then were permeabilized and blocked with 0.2% Triton X-100 (MilliporeSigma) and 3%

Table 1 | Primary antibody used in this study

Antibody	Host organism	Cat#	RRID	Vendor	Dilution	MW (kDa)	Application
NLRP3	Rabbit	ab214185	AB_2819003	Abcam	1:1000	117	WB
ASC	Rabbit	67824	AB_2799736	CST	1:1000	22	WB, IF
Caspase-1 p20	Mouse	SC-398715	AB_2819181	Santa Cruz	1:1000 for WB; 1:200 for IF	17, 40	WB, IF
IL-1β	Mouse	12242	AB_2715503	CST	1:1000	17	WB
IL-18	Rabbit	57058	NA	CST	1:1000	17, 22	WB
GSDMD	Rabbit	ab209845	AB_278550	Abcam	1:1000	32, 53	WB
HMGB1	Rabbit	3935	AB_2295241	CST	1:1000	29	WB
NF-κB p65	Rabbit	8242	AB_10859369	CST	1:1000	65	WB, IF
TNF-α	Rabbit	11948	AB_2687962	CST	1:1000	17, 25, 28	WB
IL-6	Rabbit	12912	AB_2798059	CST	1:1000	24	WB
Iba-1	Goat	ab5076	AB_2224402	Abcam	1:1000 for WB; 1:500 for IF	17	WB, IF
CD206	Mouse	SC-58986	AB_2144945	Santa Cruz	1:1000 for WB; 1:200 for IF	190	WB, IF
iNOS	Rabbit	13120	AB_2687529	CST	1:1000 for WB; 1:500 for IF	130	WB, IF
GFAP	Mouse	3670	AB_561049	CST	1:1000 for WB; 1:500 for IF	50	WB, IF
C3	Rat	NB200-540	AB_10003444	Novus Biological	1:1000 for WB; 1:500 for IF	187	WB, IF
Caspase-3	Rabbit	9662	AB_331439	CST	1:1000	17, 19, 35	WB
Bax	Rabbit	14796	AB_2716251	CST	1:1000	20	WB
NeuN	Rabbit	ab177487	AB_2532109	Abcam	1:500		IF
Ly6G	Rat	sc-53515	AB_783639	Santa Cruz	1:200		IF
F4/80	Rat	ab6640	AB_1140040	Abcam	1:500		IF

Abcam: Abcam, Cambridge, MA, USA; CST: Cell Signaling Technology, Danvers, MA, USA; IF: immunofluorescence; MW: molecular weight; NA: not applicable; Novus Biological: Novus Biological, Littleton, CO, USA; Santa Cruz: Santa Cruz Biotechnology, Santa Cruz, CA, USA; WB: western blot.

bovine serum albumin for 1.5 hours. The sections were incubated overnight at 4°C with the primary antibodies shown in **Table 1**. After washing with PBS, the sections were immersed in the corresponding Alexa Fluor-conjugated IgG (1:500, all from Thermo Fisher Scientific) for 1 hour at room temperature as follows: donkey anti-rabbit IgG, Alexa Fluor 488 (Cat# A-21206), donkey anti-rabbit IgG, Alexa Fluor 555 (Cat# A-31572), donkey anti-mouse IgG, Alexa Fluor 488 (Cat# A-21202), donkey anti-mouse IgG, Alexa Fluor 555 (Cat# A-31570), donkey anti-rat IgG, Alexa Fluor 488 (Cat# A-21208), donkey anti-goat IgG, Alexa Fluor Plus 555 (Cat# A-32816). Finally, 4′,6-diamidino-2-phenylindole (Abcam, Cambridge, UK) was applied to counterstain the nuclei. A fluorescence microscope (IX73, Olympus Corporation, Tokyo, Japan) was used to take micrographs of every slice. We captured five fields of view for every section and for each sample in the same regions of the pericontusional cortex. The number of cells and the fluorescence intensity were determined using ImageJ software (Schneider et al., 2012).

Terminal deoxynucleotidyl transferase-mediated dUTP nick-end labeling staining

We determined apoptosis of neurons in the brain tissue sections at 3 days post-TBI using an In Situ Cell Death Detection Kit (Roche, Basel, Switzerland). The mouse brain slices (*n* = 5/group) were rinsed with PBS and incubated with 0.2% Triton X-100 and 3% bovine serum albumin for 1.5 hours. Each section was stained with rabbit anti-neuronal nuclear protein antibody shown in **Table 1** overnight at 4°C. The sections were warmed to room temperature for 30 minutes and subsequently washed with PBS three times. Then, the sections were incubated with Alexa Fluor 555 donkey anti-rabbit IgG (Cat# A-31572, Thermo Fisher Scientific) and fixed with TUNEL reaction solution for 60 minutes at 37°C. The counterstaining of nuclei was conducted with 4′,6-diamidino-2-phenylindole for 5 minutes.

Hematoxylin and eosin staining and measurement of lesion volume

Lesion volume was detected as previously described (Xu et al., 2018a). After the MWM test, the mice (*n* = 6/group) were euthanized, the brains were removed and embedded in paraffin, and 5-μm coronal sections were sliced at intervals of 120 μm (approximately 25 sections/brain). For hematoxylin and eosin (H&E) staining, the sections were deparaffinized with xylene and an alcohol gradient, and the sections were counterstained with H&E (Beijing Solarbio Science & Technology Co., Ltd.) for 5 minutes. Then, the sections were dried and mounted with neutral balsam (Beijing Solarbio Science & Technology Co., Ltd.) followed by observation using a light microscope (IX73, Olympus Corporation). The volume of each tissue lesion was calculated by measuring the area of the lesion in the contralateral and ipsilateral hemispheres using ImageJ software. Then, the lesion volume (%) was calculated as follows: (interval distance × lesion volume of each section)/area of the contralateral hemisphere × 100.

Statistical analysis

No statistical methods were used to predetermine sample sizes; however, our sample sizes are similar to those reported in previous publications (Xu et al., 2018a). All data are based on at least three independent experiments. Measurement data are shown as the mean ± standard deviation (SD). All statistical analyses were performed using SPSS 22.0 software (IBM Corp. Released 2013. IBM SPSS Statistics for Windows, Version 22.0. Armonk, NY: IBM Corp.). To analyze the neurobehavioral evaluation data, two-way analysis of variance followed by Tukey's *post hoc* test was performed. Other multigroup comparisons were performed using one-way analysis of variance followed by Tukey's *post hoc* test. *P* < 0.05 was deemed statistically significant.

Results

Administration of maraviroc improves neurological functions after traumatic brain injury

All experimental designs are shown in **Figure 1A**. To investigate whether administration of maraviroc is protective in mice with TBI, we conducted mNSS tests, rotarod tests, and MWM tests. In the mNSS test, animals in the TBI + vehicle group had much higher scores than the sham group at any time point measured. Maraviroc treatment significantly alleviated the impairment of motor abilities between the third and seventh days post-TBI (**Figure 1B**), and mice in all groups reached full spontaneous recovery at 14 days post-TBI. The rotarod test results showed that the mice in the TBI + vehicle group had the worst motor coordination and balance, and mice in the TBI + maraviroc group displayed significant improvement on the third and seventh days post-TBI (**Figure 1C**). In the MWM tests, the escape latency of the TBI + vehicle group was more than the sham group, and administration of maraviroc decreased the escape latency compared with the TBI + vehicle group on days 19 and 20 (**Figure 1D**). There was no significant difference in the swim speed of all groups (**Figure 1G**). Once we removed the hidden platform at 21 days post-TBI to evaluate the number of crossings, a significant decrease in crossing number was observed in the TBI + maraviroc group compared with the TBI + vehicle group (**Figure 1E**). Furthermore, the TBI + vehicle group spent less time in the target region than the sham group, while maraviroc treatment ameliorated this phenomenon (**Figure 1F** and **I**). The mice in the maraviroc group traveled a shorter distance while searching for the platform compared with those in the TBI + vehicle group (**Figure 1H**).

Administration of maraviroc enhances tissue preservation after traumatic brain injury

At 21 days post-TBI, H&E staining of brain tissue showed that the sham group had no gross lesion to the cortex, while noticeable damage was observed in the TBI + vehicle group. The TBI + maraviroc group had more tissue preservation than the TBI + vehicle group (**Figure 1J** and **K**).

Administration of maraviroc regulates microglial polarization and reduces neutrophil and macrophage infiltration after traumatic brain injury

Microglia convert from the resting type into the M1 and M2 phenotypes after TBI; this process plays a vital role in the neuroinflammatory response (Long et al., 2020). To determine the effect of maraviroc on microglial polarization, coimmunofluorescence staining of a panmicroglial marker (ionized calcium-binding adapter molecule 1 [Iba-1]), an M1 microglial marker (inducible nitric oxide synthase [iNOS]), and an M2 microglial marker (macrophage mannose receptor 1 [CD206]) was performed to determine the shifts in microglial polarization 3 days after TBI. Maraviroc administration remarkably decreased the number of Iba-1-positive cells that also expressed iNOS and increased the expression of CD206 in the perilesional area, indicating an M1-to-M2 microglial transition (**Figure 2A–D**). Furthermore, western blot analysis at 3 days post-TBI in the lesioned cortex showed that iNOS expression was inhibited and CD206 expression was significantly increased after maraviroc administration. However, the protein expression level of Iba-1 in tissues from mice in the maraviroc treatment group did not significantly differ from that in mice in the vehicle treatment group (**Figure 2E–H**). In addition, immunofluorescence staining showed the accumulation of adhesion G protein-coupled receptor E1 (cell surface glycoprotein F4/80 [F4/80])-positive and lymphocyte antigen 6G (Ly-6G)-positive cells in the pericontusional region in the TBI + vehicle group compared with that in the TBI + maraviroc group at 3 days post-TBI (**Figure 3A–D**).
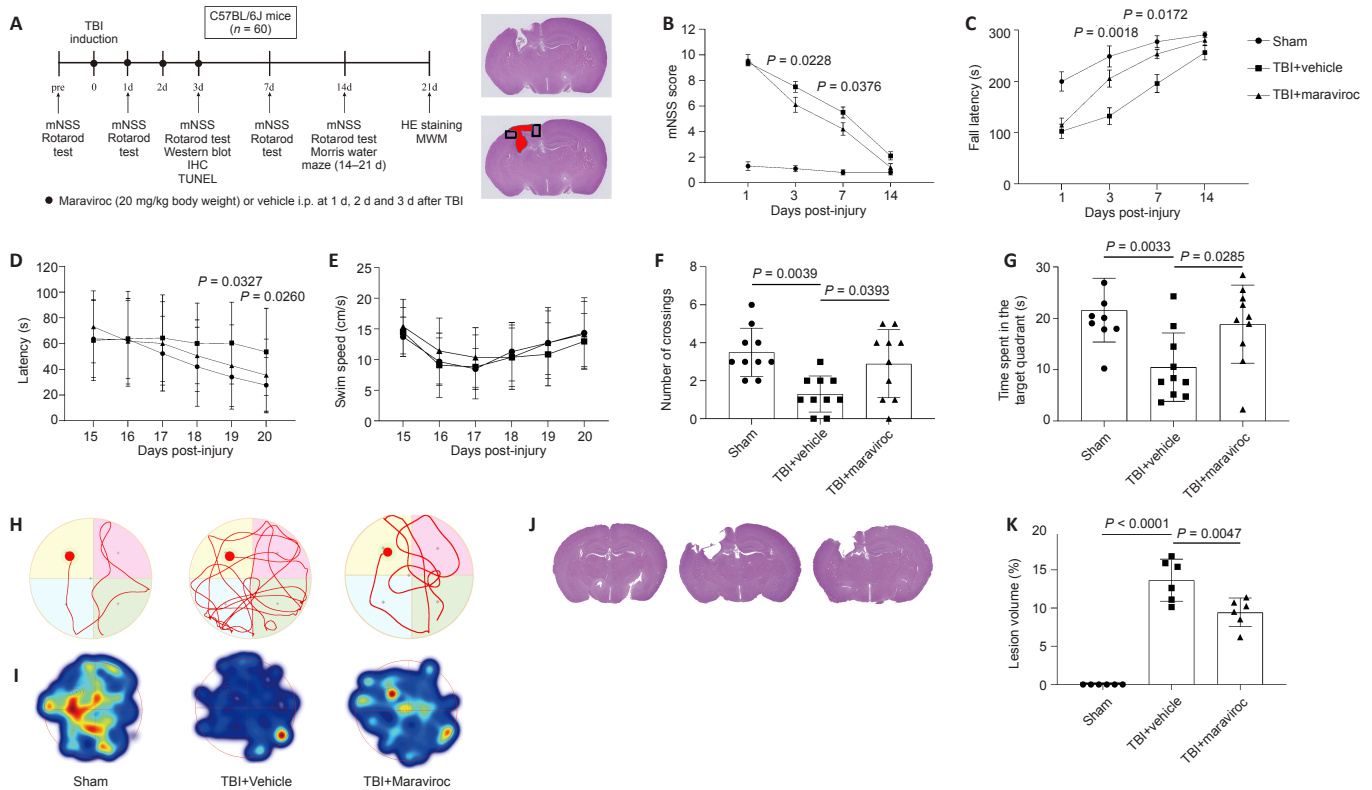
Figure 1 | Neuroprotective effect of maraviroc on neurological function and cortical lesion size after traumatic brain injury.
(A) Experimental design. The black boxes in the H&E-stained illustration show the perilesional cortex, and the red region shows the lesioned area. (B–G) Neurological performance was assessed by the mNSS score (B), rotarod tests (C), and MWM tests (D–G). Representative heatmap of swimming traces (H) and thermal imaging of the probe trial (I) at 21 days post-TBI. The red circle in Figure 1H indicates the location of the platform in the MWM test. (J) Representative H&E-stained images of the brain slices of each group, and (K) quantitative analysis of the lesioned area volume at 21 days post-TBI. P-values shown in B–D represent the statistical significance between the TBI + maraviroc and TBI + vehicle groups. Two-way analysis of variance followed by Tukey's *post hoc* test was performed to analyze the neurobehavioral evaluation data in B–G. One-way analysis of variance followed by Tukey's *post hoc* test was used in K. Data are shown as the mean ± SD. The sample size was n = 10/group for neurological function assessment and n = 6/group for H&E staining. All experiments were repeated at least three times. H&E: Hematoxylin and eosin; IHC: immunohistochemistry; i.p.: intraperitoneally; mNSS: modified neurological severity score; MWM: Morris water maze; TBI: traumatic brain injury.
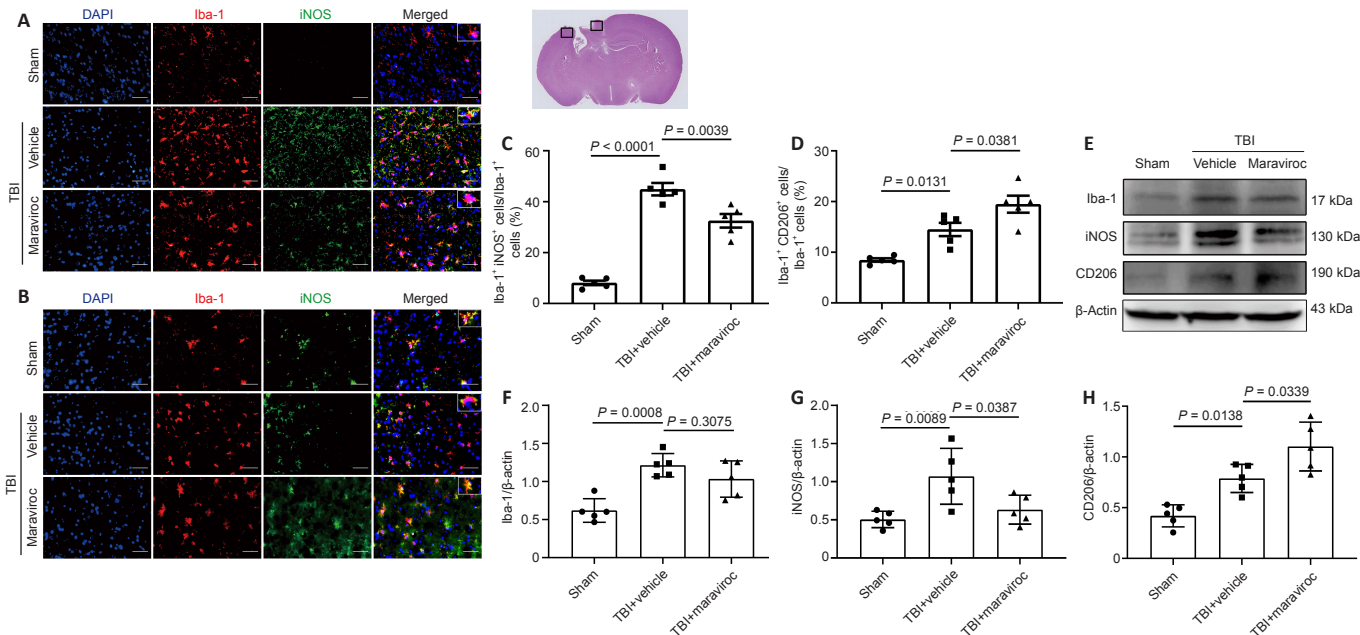
Figure 2 | Effect of maraviroc on microglial activation and polarization in the perilesional cortex area of mice after traumatic brain injury.
(A, B) Representative immunofluorescence staining photographs of iNOS (green, A) and CD206 (green, B) in Iba-1-positive cells (red) in the perilesional cortex on the third day post-TBI. Scale bar: 50 μm. (C, D) Quantitative data corresponding to A and B. Maraviroc administration significantly decreased the number of iNOS-positive M1 microglia (P = 0.0039) and increased the expression of CD206-positive microglia (P = 0.0381) in the perilesional area compared with those in the TBI + vehicle group. The black boxes in the hematoxylin and eosin-stained illustration show the perilesional cortex. (E–H) Representative western blot results of Iba-1 (F), iNOS (G), and CD206 (H) at 3 days post-TBI. Administration of maraviroc decreased the expression level of iNOS (P = 0.0387) and increased the expression level of CD206 (P = 0.0339) but did not alter the protein level of Iba-1. One-way analysis of variance followed by the Tukey's *post hoc* test was used. Data are expressed as the mean ± SD (n = 5/group). All experiments were repeated at least three times. DAPI: 4′,6-Diamidino-2-phenylindole; iNOS: inducible nitric oxide synthase; TBI: traumatic brain injury.
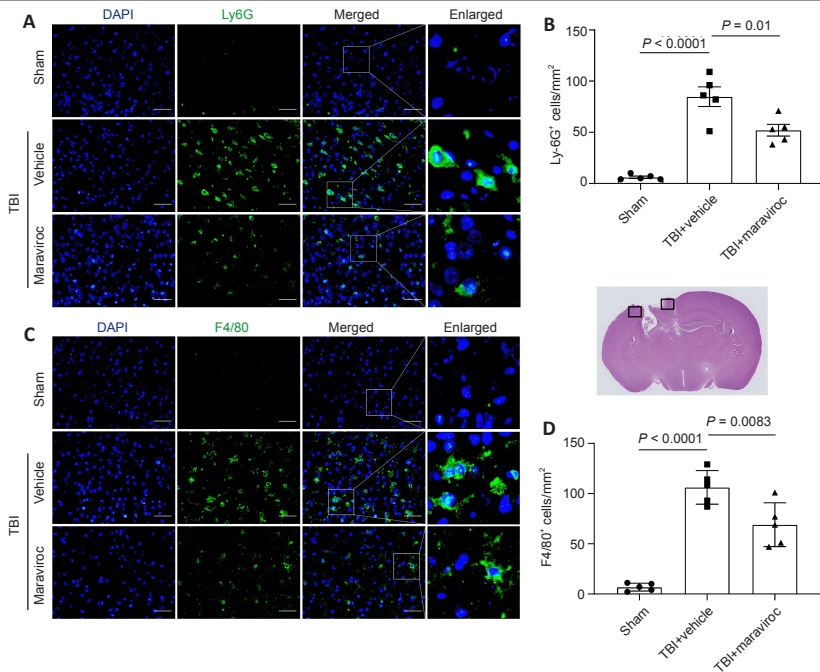
Figure 3 | Effect of maraviroc on neutrophil and macrophage infiltration after traumatic brain injury.
(A–D) Representative immunofluorescence staining micrographs of Ly-6G (green, A) and F4/80 (green, C) in the perilesional cortex at 3 days post-TBI. Scale bars: 50 μm. (B, D) Maraviroc decreased the number of Ly-6G-positive (P = 0.01) (B) and F4/80-positive (P = 0.0083) (D) cells after traumatic brain injury. The black boxes in the hematoxylin and eosin-stained illustration show the perilesional cortex. One-way analysis of variance followed by Tukey's *post hoc* test was used. Data are expressed as the mean ± SD (n = 5/ group). All experiments were repeated at least three times. DAPI: 4′,6-Diamidino-2-phenylindole; F4/80: adhesion G protein-coupled receptor E1 (cell surface glycoprotein F4/80); Ly-6G: lymphocyte antigen 6G.

Administration of maraviroc inhibits the HMGB1/NF-κB pathway and alters the inflammatory response in the pericontusional cortex after traumatic brain injury

High mobility group protein B1 (HMGB1) translocation and release have been shown to activate microglia and exacerbate neuroinflammation induced by TBI (Paudel et al., 2020). The nuclear factor kappa B (NF-κB) pathway is related to high expression levels of HMGB1 and the subsequent release of inflammatory factors. The HMGB1/NF-κB pathway may play a critical role in the pathological process of TBI (Chen et al., 2018). Western blot analysis illustrated that the expression levels of HMGB1 and NF-κB p65 in the lesioned cortex were significantly increased at 3 days after TBI (**Figure 4A**, **E**, and **F**). In contrast, administration of maraviroc effectively decreased HMGB1 and NF-κB p65 protein expression compared with vehicle treatment after TBI. Moreover, a western blot assay of proinflammatory cytokine levels showed that maraviroc treatment significantly inhibited the expression of these inflammatory factors compared with vehicle treatment after TBI (**Figure 4A–D**). Immunofluorescence staining further demonstrated that the TBI + maraviroc group had a significantly reduced percentage of cells with nuclei that stained positive for NF-κB p65 compared with that in the TBI + vehicle group (**Figure 4G** and **H**).
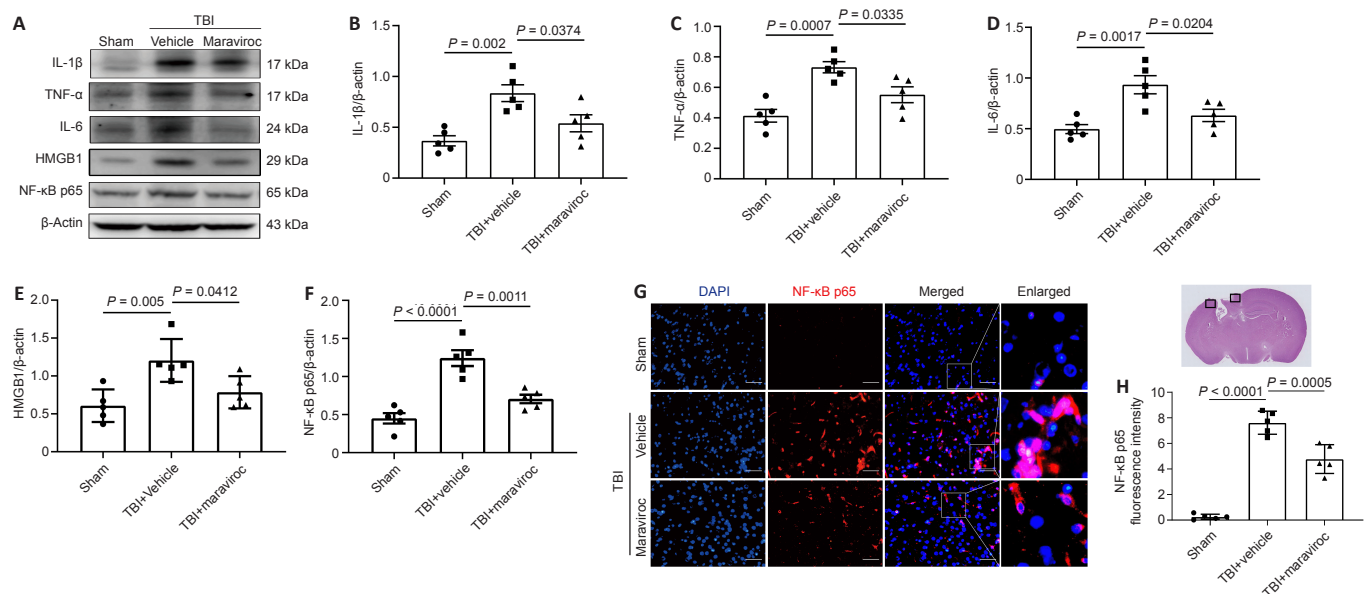
Figure 4 | Effect of maraviroc on the HMGB1/NF-κB pathway and inflammatory cytokines in the perilesional cortex after traumatic brain injury.
(A–F) Representative western blot bands and quantitative data of IL-1β (B), TNF-α (C), IL-6 (D), HMGB1 (E), and NF-κB p65 (F) protein expression in the perilesional cortex 3 days post-TBI. (G, H) Representative photographs of immunofluorescence staining of NF-κB p65 in the perilesional cortex at 3 days post-TBI. Scale bars: 50 μm. Maraviroc treatment alleviated neuroinflammation post-TBI compared with the TBI + vehicle group (P = 0.0005). The black boxes in the hematoxylin and eosin-stained illustration show the perilesional cortex. One-way analysis of variance followed by Tukey's *post hoc* test was used. Data are expressed as the mean ± SD (n = 5/group). All experiments were repeated at least three times. DAPI: 4′,6-Diamidino-2-phenylindole; HMGB1: high mobility group protein B1; IL: interleukin; NF-κB: nuclear factor NF-kappa-B; TBI: traumatic brain injury; TNF: tumor necrosis factor.

Administration of maraviroc suppressed NLRP3 inflammasome activation after traumatic brain injury

Western blotting and immunofluorescence were conducted to determine the NLRP3 inflammasome expression levels among different groups. The TBI + vehicle group had elevated levels of NLRP3, caspase-1 p20, apoptotic speck-containing protein, IL-18, IL-1β, and gasdermin-D compared with the sham group (**Figure 5A–G**). The TBI + maraviroc group had significantly decreased protein levels of the NLRP3 inflammasome compared with the TBI + vehicle group. In addition, immunofluorescence analysis revealed that the elevated caspase-1 p20 immunoreactivity in the pericontusional cortex was greatly alleviated by maraviroc administration compared with vehicle administration

(**Figure 5H** and **I**).

Administration of maraviroc decreased the activation of neurotoxic reactive astrocytes

We estimated whether maraviroc treatment suppressed neurotoxic reactive astrocytes using immunohistochemical and western blot assays. The expression levels of glial fibrillary acidic protein (GFAP) were significantly increased in the TBI + vehicle group in the ipsilateral hemisphere compared with the sham group (P = 0.0091), but there was no difference between the TBI + vehicle group and the TBI + maraviroc group (P = 0.3987; **Figure 6A** and **B**). However, we observed that the protein levels of the neurotoxic reactive

astrocyte-associated marker complement C3 were elevated in the vehicle-treated group compared with the sham group and decreased after maraviroc administration (**Figure 6C**). Coimmunofluorescence revealed that the maraviroc treatment group exhibited a notable decline in the number of C3-positive and GFAP-positive astrocytes compared with the vehicle treatment group in the lesioned cortex 3 days post-TBI (**Figure 6D** and **E**).

Administration of maraviroc protects neurons against traumatic brain injury-induced neuronal apoptosis

Excessively activated inflammatory responses, NLRP3 inflammasomes, and A1

astrocytes are closely related to the prevalence of apoptosis (Liu et al., 2013; Roth et al., 2014; Liddelow et al., 2017; Skelly et al., 2019). We estimated the effect of maraviroc on neural cell death at 3 days post-TBI, and western blotting analyses were performed to quantify apoptotic cells. Maraviroc administration decreased the levels of cleaved caspase-3 and the apoptosis regulator BAX compared with vehicle administration (**Figure 7A** and **B**). In addition, double staining with the TUNEL assay and neuronal nuclear protein revealed many more apoptotic cells in the vehicle treatment group than in the sham group, but maraviroc treatment significantly decreased the apoptotic index compared with vehicle treatment (**Figure 7C–E**).
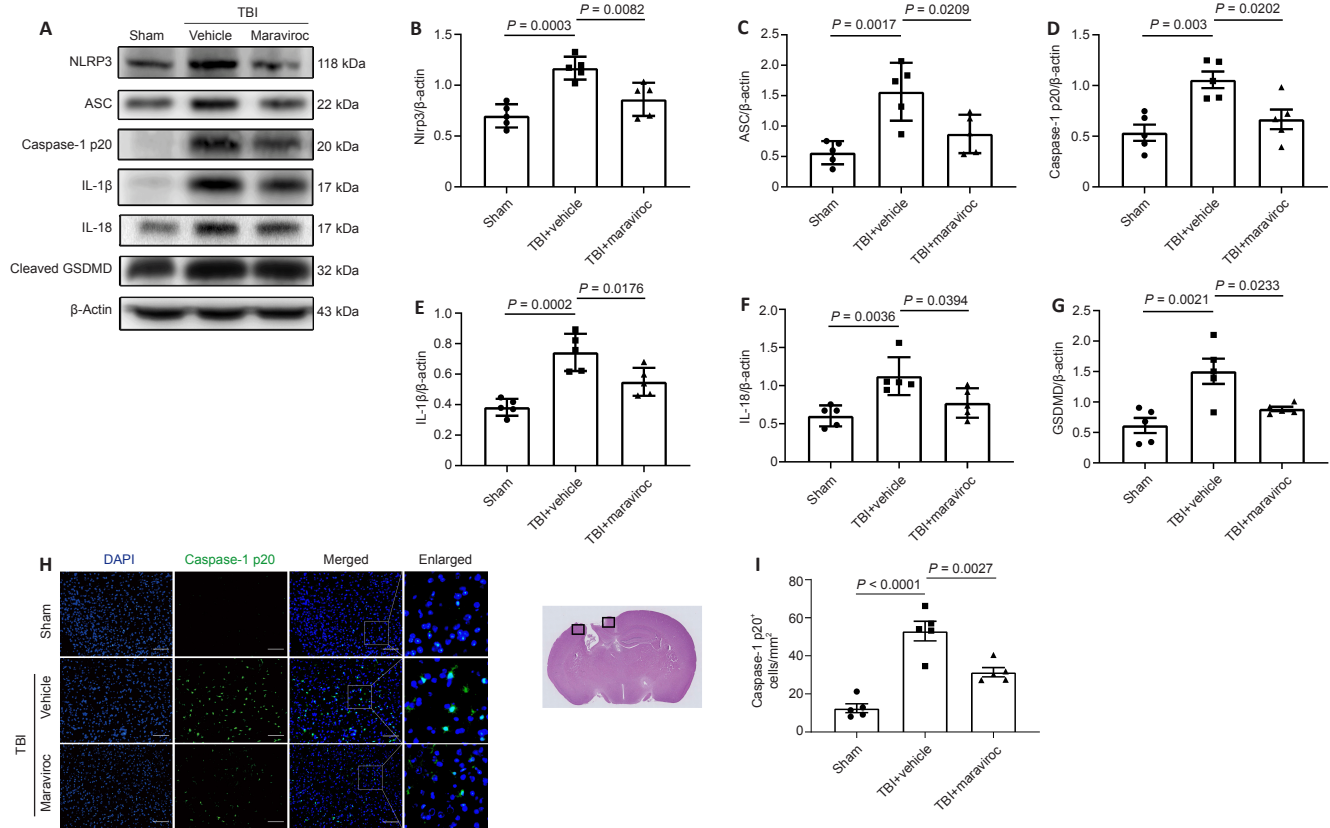
Figure 5 | Effect of maraviroc on the expression of the NLRP3 inflammasome after traumatic brain injury.
(A–G) Representative western blot bands and quantitative data of NLRP3 (B), ASC (C), cleaved caspase-1 p20 (D), IL-1β (E), IL-18 (F), and cleaved GSDMD (G) in the pericontusional cerebral cortex 3 days post-TBI. Maraviroc treatment alleviated the TBI-induced activation of NLRP3 inflammasome components and substrates at 3 days postinjury compared with the TBI + vehicle group (P = 0.0082 for B, P < 0.05 for C–G). (H–I) Representative immunofluorescence staining micrographs for caspase-1 p20 (green) in the perilesional cortex at 3 days post-TBI. The black boxes in the hematoxylin and eosin-stained illustration show the perilesional cortex. Scale bars: 100 μm. Maraviroc treatment significantly decreased the number of caspase-1 p20-positive cells compared with the TBI + vehicle group (P = 0.0027). One-way analysis of variance followed by Tukey's *post hoc* test was used. Data are shown as the mean ± SD (n = 5/group). All experiments were repeated at least three times. ASC: Apoptosis-associated speck-like protein containing a CARD; DAPI: 4′,6-diamidino-2-phenylindole; GSDMD: gasdermin-D; IL: interleukin; NLRP3: NACHT, LRR, and PYD domains-containing protein 3; TBI: traumatic brain injury.
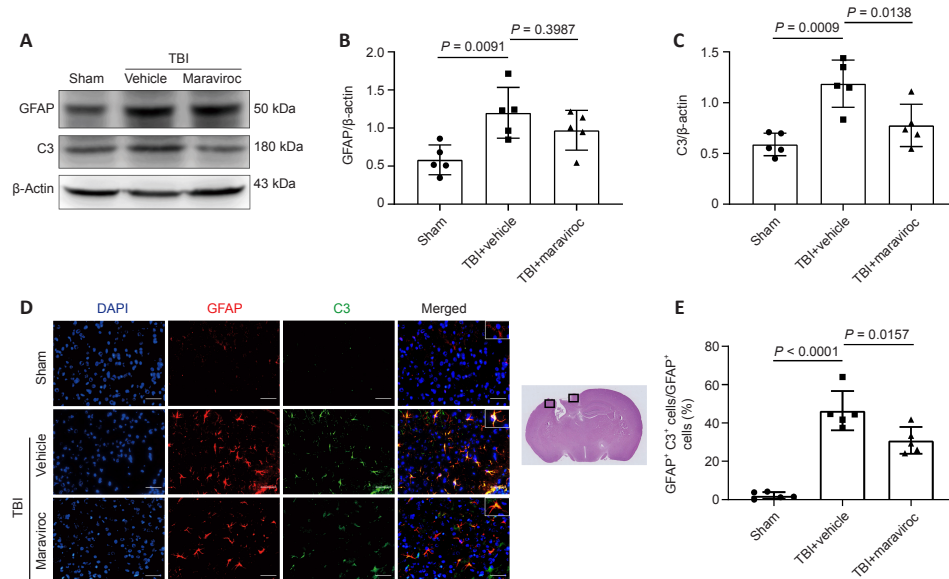
Figure 6 | Effect of maraviroc on neurotoxic reactive astrocyte activation in the pericontusional cortex of mice with traumatic brain injury.
(A–C) Representative immunoblot bands and quantitative data of GFAP (B) and C3 (C) 3 days post-TBI. Maraviroc administration significantly decreased C3 protein expression after TBI (P = 0.0138). (D–E) Representative double immunofluorescence staining photographs and corresponding quantitative data for complement C3 (green) and GFAP (red) in the perilesional cortex at 3 days post-TBI. Maraviroc administration significantly decreased the activation of neurotoxic reactive astrocytes in the perilesional cortex at 3 days post-TBI (P = 0.0157). The black boxes in the hematoxylin and eosin-stained illustration show the perilesional cortex. Scale bars: 50 μm. One-way analysis of variance followed by the Tukey's *post hoc* test was used. Data are expressed as the mean ± SD (n = 5/group). All experiments were repeated at least three times. DAPI: 4′,6-Diamidino-2-phenylindole; GFAP: glial acidic fibrillary protein; C3: complement C3; TBI: traumatic brain injury.
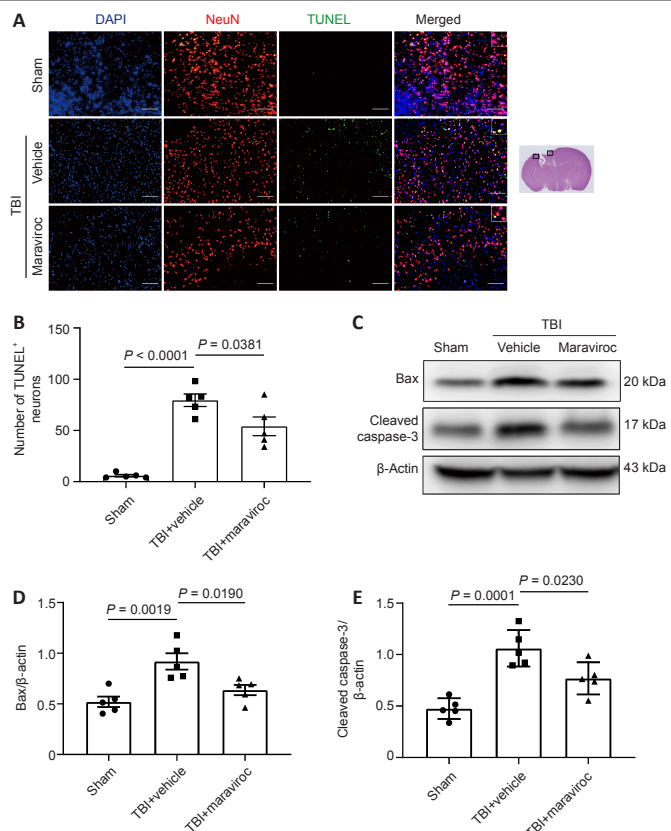
Figure 7 | Effect of maraviroc on neuronal apoptosis at 3 days after traumatic brain injury.

(A, B) Representative micrographs of immunostaining and corresponding quantification data of TUNEL-positive neurons. Scale bars: 100 μm. The number of TUNEL-positive neurons was significantly decreased in the maraviroc administration group compared with the vehicle + TBI group in the perilesional region ($P = 0.0381$). The black boxes in the hematoxylin and eosin-stained illustration show the perilesional cortex. (C–E) Representative western blot bands and corresponding quantification data of BAX (D) and cleaved caspase-3 (E) in the perilesional cortex at 3 days post-TBI. Maraviroc administration significantly decreased the protein expression of BAX ($P = 0.0190$) and cleaved caspase-3 ($P = 0.0230$) compared with the TBI + vehicle group. One-way analysis of variance followed by Tukey's *post hoc* test was used. All the results were shown as the mean ± SD ($n = 5$/group). All experiments were repeated at least three times. DAPI: 4′,6-Diamidino-2-phenylindole; NeuN: neuronal nuclear protein; TBI: traumatic brain injury; TUNEL: terminal deoxynucleotidyl transferase-mediated biotin-deoxyuridine triphosphate nick-end labeling.

Discussion

The major points of our present study are as follows: administration of maraviroc, an U.S. Food and Drug Administration-approved drug, alleviated neurological deficits and resulted in neurological function recovery after TBI; maraviroc treatment enhanced tissue preservation after TBI; maraviroc treatment regulated microglial polarization, reduced neutrophil and macrophage infiltration and NLRP3 inflammasome activation, and inhibited the HMGB1/NF-κB pathway and subsequent release of inflammatory factors after TBI; and maraviroc treatment inhibited neuronal apoptosis and reduced complement C3 and caspase-3 expression levels.

Neuroinflammation exerts a vital effect on the physiological process of TBI (Morganti-Kossmann et al., 2019). At the early stage of TBI, resident microglia are activated, and peripheral neutrophils are recruited to the perilesional cortex. Subsequently, chemokine signaling causes the recruitment and infiltration of immunocytes into the lesioned cortex (Jassam et al., 2017). Meanwhile, inflammatory cytokines, such as TNF-α, IL-1β, and IL-6, are released by these immunocytes. Excessive posttraumatic neuroinflammation contributes to secondary brain damage and neuronal cell death in the perilesional cortex and hippocampus and exacerbates neurological dysfunctions (Morganti-Kossmann et al., 2019). Microglia rapidly respond to brain injury and are then recruited to the pericontusional cortex and release inflammatory cytokines, ultimately resulting in axonal injury and neuronal cell death after TBI (Witcher et al., 2015). Moreover, activated microglia polarize from the proinflammatory M1 subtype to the anti-inflammatory M2 subtype to regulate neuroinflammation (Wang et al., 2013; Hu et al., 2015). M1 microglia infiltrate lesioned cortex areas at 7 days poststroke, and M2 microglia are the main subtype present at 3 days poststroke (Xiong et al., 2016). Ample evidence indicates that knocking out or pharmacologically inhibiting CCR5 suppresses the inflammatory response

by alleviating leukocyte, T cell, and macrophage infiltration and by promoting M2 macrophage activation (Glass et al., 2005; Rosi et al., 2005; Arberas et al., 2013; Long et al., 2020). Our study demonstrated that maraviroc could decrease neutrophil and macrophage infiltration and proneuroinflammatory cytokine release. Furthermore, we expand the notion that maraviroc treatment encourages a shift from M1 microglia toward M2 microglia to inhibit progressive inflammation and the destruction of the lesioned cortex 3 days post-TBI.

NLRP3 inflammasome activation leads to cleavage of the precursor form of caspase-1, the release of IL-1β and IL-18, and the induction of neuronal degradation (Feng et al., 2021). Recently, the proinflammatory effects of the NLRP3 inflammasome in stroke, multiple sclerosis, Alzheimer's disease, Parkinson's disease, and TBI have been described (Heneka et al., 2013; Ren et al., 2018; Malhotra et al., 2020; Kwon et al., 2021). Thus, the therapeutic strategy targeting the NLRP3 inflammasome could potentially improve neurological outcomes after TBI. As shown in our studies, the expression levels of pyroptosis-related proteins were higher in the lesioned cortex of mice subjected to TBI. In contrast, maraviroc treatment significantly decreased the levels of these proteins. HMGB1, an endogenous damage-associated molecule widely expressed in microglia, exerts a proinflammatory effect (Lee et al., 2014). Binding of HMGB1 to toll-like receptor 4 and advanced glycosylation end product-specific receptor activates p38 and NF-κB to amplify the inflammatory response. Recent studies have shown that activation of the HMGB1/toll-like receptor 4 or HMGB1/advanced glycosylation end product-specific pathways results in the activation of NF-κB to exacerbate the inflammatory cascade (Crews et al., 2013; Jia et al., 2019). In addition, several studies have illustrated that activation of NLRP3 is triggered by HMGB1, which leads to pyroptosis-mediated cell death in endothelial cells and acute pancreatitis (Jia et al., 2019; Wu et al., 2021). Our study demonstrates that maraviroc mitigates the protein levels of HMGB1 and NF-κB in the perilesional cortex at 3 days post-TBI and is the first study, to our knowledge, that links CCR5 receptor inhibition to the HMGB1/NF-κB/NLRP3 pathway.

Astrocytes are widely distributed in the mammalian CNS and perform numerous essential functions. Astrocytes undergo a process called astrogliosis to become "reactive astrocytes" in reaction to CNS injury (Zamanian et al., 2012). Previous studies reported that reactive astrocytes restrict neuroinflammation, BBB repair, neuronal protection, and neurologic function recovery (Sofroniew, 2015; Almad and Maragakis, 2018; Göbel et al., 2020). However, reactive astrocytes can exert negative effects, such as aggravating inflammation or interfering with axon growth (Silver and Miller, 2004). Recently, a study demonstrated that reactive astrocytes were polarized into neurotoxic reactive astrocytes (A1 astrocytes) and neuroprotective reactive astrocytes (A2 astrocytes) in response to neuroinflammation and ischemia, respectively (Liddelow et al., 2017). IL-1α, TNF-α, and complement C1q are released by activated microglia, causing the activation of A1 astrocytes in CNS injuries and diseases, such as Alzheimer's disease, Parkinson's disease, stroke, and TBI (Goetzl et al., 2018; Yun et al., 2018; Clark et al., 2019; Cao et al., 2021). A1 astrocytes lose their fundamental functions and exert neurotoxic functions, such as inducing the death of neuronal cells and mature oligodendrocytes (Liddelow et al., 2017). Neurotoxic reactive astrocytes that highly expressed complement C3 play neurotoxic roles in CNS diseases by releasing very-long-chain fatty acid acyl chains and free fatty acids (Escartin et al., 2021). Targeting neurotoxic reactive astrocytes may be a potential approach to promote the preservation of neuronal cells. In our study, we demonstrated that maraviroc had no effect on the activation of astrocytes or GFAP expression in the ipsilateral hemisphere. However, maraviroc induced a significant reduction in complement C3, which is a neurotoxic reactive astrocyte marker, in the pericontusional cortex 3 days postinjury. Double immunofluorescence staining of GFAP and complement C3 confirmed that maraviroc inhibits A1 astrocyte activation. The NF-κB signaling pathway is involved in physiopathological processes after TBI, such as neuroinflammatory reactivity in astrocytes and microglia and cell survival. Furthermore, downregulation of NF-κB and upregulation of phosphatidylinositol 3-kinase/protein kinase B regulates the shift from the A1 to the A2 phenotype (Xu et al., 2018b). Notably, our results suggest that maraviroc might suppress neurotoxic reactive astrocyte alterations by regulating the NF-κB pathway. To the best of our knowledge, our study illustrates for the first time that maraviroc exerts a neuroprotective role by modulating neurotoxic reactive astrocyte activation and reducing neuronal cell loss.

Maraviroc is the primary CCR5 antagonist licensed by the U.S. Food and Drug Administration and has been considered a novel therapy in various neuroinflammatory diseases except for human immunodeficiency virus treatment. A study demonstrated that CCR5 plays a crucial role in HIV infection and pathogenesis because CCR5delta32, a mutant allele of the CCR5 gene, confers relative resistance to HIV infection (Dean et al., 1996). The identification of CCR5delta32 promoted the discovery and development of CCR5 inhibitors, such as maraviroc (Xu et al., 2014). Ample evidence has confirmed that maraviroc contributes to neurological function recovery after CNS injuries. A recent study demonstrated that people carrying the CCR5delta32 mutation have better cognitive function after stroke (Joy et al al., 2019). However, the neuroprotective role of maraviroc in TBI mediated by inhibition of NLRP3 inflammasome activation has not been revealed to date. Our results first confirmed that administration of maraviroc attenuated neuroinflammation by regulating microglial polarization and reducing neutrophil infiltration, inflammatory cytokine production, and the activation

of the HMGB1/NF-κB/NLRP3 pathway after TBI. Furthermore, maraviroc administration protected neuronal cells against apoptosis by decreasing the expression of caspase-3 and BAX. Maraviroc administration also inhibited neurotoxic reactive astrocyte activation and the caspase-3 pathway to exert antiapoptotic effects.

Neurologic dysfunction, including short-term neurologic dysfunction and long-term cognitive dysfunction, is common after brain injury, and more than half of patients with TBI experience TBI-induced chronic cognitive impairment (Rabinowitz and Levin, 2014). TBI induces the apoptosis of hippocampal neurons, which is responsible for cognitive deficits in the chronic postinjury phase (Yang et al., 2016). Our findings reveal that maraviroc treatment promotes the survival of neurons by inhibiting neuroinflammation, caspase-3 expression, and neurotoxic reactive astrocyte activation and improves cognitive function recovery after TBI.

Our study had some limitations. We only focused on the potential anti-inflammatory effects of maraviroc without investigating its effects on BBB leakage and endothelial dysfunction following TBI. Further studies are required to determine the effects of maraviroc on BBB function after TBI.

In summary, our study provides compelling evidence that maraviroc could attenuate neuroinflammation and regulate the polarization of microglia and astrocytes after TBI via pharmacological blockade of the CCR5 receptor. Thus, the CCR5 receptor might be a promising pharmacotherapeutic target after TBI.

References

Almad A, Maragakis NJ (2018) A stocked toolbox for understanding the role of astrocytes in disease. Nat Rev Neurol 14:351-362.

Arberas H, Guardo AC, Bargalló ME, Maleno MJ, Calvo M, Blanco JL, García F, Gatell JM, Plana M (2013) In vitro effects of the CCR5 inhibitor maraviroc on human T cell function. J Antimicrob Chemother 68:577-586.

Cao J, Dong L, Luo J, Zeng F, Hong Z, Liu Y, Zhao Y, Xia Z, Zuo D, Xu L, Tao T (2021) Supplemental N-3 polyunsaturated fatty acids limit A1-specific astrocyte polarization via attenuating mitochondrial dysfunction in ischemic stroke in mice. Oxid Med Cell Longev 2021:5524705.

Chen W, Guo C, Huang S, Jia Z, Wang J, Zhong J, Ge H, Yuan J, Chen T, Liu X, Hu R, Yin Y, Feng H (2020) MitoQ attenuates brain damage by polarizing microglia towards the M2 phenotype through inhibition of the NLRP3 inflammasome after ICH. Pharmacol Res 161:105122.

Chen X, Chen C, Fan S, Wu S, Yang F, Fang Z, Fu H, Li Y (2018) Omega-3 polyunsaturated fatty acid attenuates the inflammatory response by modulating microglia polarization through SIRT1-mediated deacetylation of the HMGB1/NF-κB pathway following experimental traumatic brain injury. J Neuroinflammation 15:116.

Chen X, Gao C, Yan Y, Cheng Z, Chen G, Rui T, Luo C, Gao Y, Wang T, Chen X, Tao L (2021) Ruxolitinib exerts neuroprotection via repressing ferroptosis in a mouse model of traumatic brain injury. Exp Neurol 342:113762.

Clark DPQ, Perreau VM, Shultz SR, Brady RD, Lei E, Dixit S, Taylor JM, Beart PM, Boon WC (2019) Inflammation in traumatic brain injury: roles for toxic A1 astrocytes and microglial-astrocytic crosstalk. Neurochem Res 44:1410-1424.

Corps KN, Roth TL, McGavern DB (2015) Inflammation and neuroprotection in traumatic brain injury. JAMA Neurol 72:355-362.

Crews F, Qin L, Sheedy D, Vetreno R, Zou J (2013) High mobility group box 1/Toll-like receptor danger signaling increases brain neuroimmune activation in alcohol dependence. Biol Psychiatry 73:602-612.

Dean M, Carrington M, Winkler C, Huttley GA, Smith MW, Allikmets R, Goedert JJ, Buchbinder SP, Vittinghoff E, Gomperts E, Donfield S, Vlahov D, Kaslow R, Saah A, Rinaldo C, Detels R, O'Brien SJ (1996) Genetic restriction of HIV-1 infection and progression to AIDS by a deletion allele of the CKR5 structural gene. Hemophilia Growth and Development Study, Multicenter AIDS Cohort Study, Multicenter Hemophilia Cohort Study, San Francisco City Cohort, ALIVE Study. Science 273:1856-1862.

Diaz-Castro B, Gangwani MR, Yu X, Coppola G, Khakh BS (2019) Astrocyte molecular signatures in Huntington's disease. Sci Transl Med 11:eaaw8546.

Escartin C, Galea E, Lakatos A, O'Callaghan JP, Petzold GC, Serrano-Pozo A, Steinhäuser C, Volterra A, Carmignoto G, Agarwal A, Allen NJ, Araque A, Barbeito L, Barzilai A, Bergles DE, Bonvento G, Butt AM, Chen WT, Cohen-Salmon M, Cunningham C, et al. (2021) Reactive astrocyte nomenclature, definitions, and future directions. Nat Neurosci 24:312-325.

Feng X, Zhan F, Luo D, Hu J, Wei G, Hua F, Xu G (2021) LncRNA 4344 promotes NLRP3-related neuroinflammation and cognitive impairment by targeting miR-138-5p. Brain Behav Immun 98:283-298.

Franke M, Bieber M, Kraft P, Weber ANR, Stoll G, Schuhmann MK (2021) The NLRP3 inflammasome drives inflammation in ischemia/reperfusion injury after transient middle cerebral artery occlusion in mice. Brain Behav Immun 92:223-233.

Friedman-Levi Y, Liraz-Zaltsman S, Shemesh C, Rosenblatt K, Kesner EL, Gincberg G, Carmichael ST, Silva AJ, Shohami E (2021) Pharmacological blockers of CCR5 and CXCR4 improve recovery after traumatic brain injury. Exp Neurol 338:113604.

Glass WG, Lim JK, Cholera R, Pletnev AG, Gao JL, Murphy PM (2005) Chemokine receptor CCR5 promotes leukocyte trafficking to the brain and survival in West Nile virus infection. J Exp Med 202:1087-1098.

Goetzl EJ, Schwartz JB, Abner EL, Jicha GA, Kapogiannis D (2018) High complement levels in astrocyte-derived exosomes of Alzheimer disease. Ann Neurol 83:544-552.

Göbel J, Engelhardt E, Pelzer P, Sakthivelu V, Jahn HM, Jevtic M, Folz-Donahue K, Kukat C, Schauss A, Frese CK, Giavalisco P, Ghanem A, Conzelmann KK, Motori E, Bergami M (2020) Mitochondria-endoplasmic reticulum contacts in reactive astrocytes promote vascular remodeling. Cell Metab 31:791-808.e8.

Heneka MT, Kummer MP, Stutz A, Delekate A, Schwartz S, Vieira-Saecker A, Griep A, Axt D, Remus A, Tzeng TC, Gelpi E, Halle A, Korte M, Latz E, Golenbock DT (2013) NLRP3 is activated in Alzheimer's disease and contributes to pathology in APP/PS1 mice. Nature 493:674-678.

Hu X, Leak RK, Shi Y, Suenaga J, Gao Y, Zheng P, and Chen J (2015) Microglial and macrophage polarization—new prospects for brain repair. Nat Rev Neurol 11:56-64.

Ismail H, Shakkour Z, Tabet M, Abdelhady S, Kobaisi A, Abedi R, Nasrallah L, Pintus G, Al-Dhaheri Y, Mondello S, El-Khoury R, Eid AH, Kobeissy F, Salameh J (2020) Traumatic brain injury: oxidative stress and novel anti-oxidants such as mitoquinone and edaravone. Antioxidants (Basel) 9:943.

Jassam YN, Izzy S, Whalen M, McGavern DB, El Khoury J (2017) Neuroimmunology of traumatic brain injury: time for a paradigm shift. Neuron 95:1246-1265.

Jia C, Zhang J, Chen H, Zhuge Y, Chen H, Qian F, Zhou K, Niu C, Wang F, Qiu H, Wang Z, Xiao J, Rong X, Chu M (2019) Endothelial cell pyroptosis plays an important role in Kawasaki disease via HMGB1/RAGE/cathespin B signaling pathway and NLRP3 inflammasome activation. Cell Death Dis 10:778.

Johnson VE, Weber MT, Xiao R, Cullen DK, Meaney DF, Stewart W, and Smith DH (2018) Mechanical disruption of the blood-brain barrier following experimental concussion. Acta Neuropathol 135:711-726.

Joy MT, Ben Assayag E, Shabashov-Stone D, Liraz-Zaltsman S, Mazzitelli J, Arenas M, Abduljawad N, Kliper E, Korczyn AD, Thareja NS, Kesner EL, Zhou M, Huang S, Silva TK, Katz N, Bornstein NM, Silva AJ, Shohami E, Carmichael ST (2019) CCR5 is a therapeutic target for recovery after stroke and traumatic brain injury. Cell 176:1143-1157.e13.

Kwon OC, Song JJ, Yang Y, Kim SH, Kim JY, Seok MJ, Hwang I, Yu JW, Karmacharya J, Maeng HJ, Kim J, Jho EH, Ko SY, Son H, Chang MY, Lee SH (2021) SGK1 inhibition in glia ameliorates pathologies and symptoms in Parkinson disease animal models. EMBO Mol Med 13:e13076.

Lee S, Nam Y, Koo J, Lim D, Park J, Ock J, Kim J, Suk K, Park S (2014) A small molecule binding HMGB1 and HMGB2 inhibits microglia-mediated neuroinflammation. Nat Chem Biol 10:1055-1060.

Liddelow SA, Guttenplan KA, Clarke LE, Bennett FC, Bohlen CJ, Schirmer L, Bennett ML, Münch AE, Chung WS, Peterson TC, Wilton DK, Frouin A, Napier BA, Panicker N, Kumar M, Buckwalter MS, Rowitch DH, Dawson VL, Dawson TM, Stevens B, et al. (2017) Neurotoxic reactive astrocytes are induced by activated microglia. Nature 541:481-487.

Liu HD, Li W, Chen ZR, Hu YC, Zhang DD, Shen W, Zhou ML, Zhu L, Hang CH (2013) Expression of the NLRP3 inflammasome in cerebral cortex after traumatic brain injury in a rat model. Neurochem Res 38:2072-2083.

Long X, Yao X, Jiang Q, Yang Y, He X, Tian W, Zhao K, Zhang H (2020) Astrocyte-derived exosomes enriched with miR-873a-5p inhibit neuroinflammation via microglia phenotype modulation after traumatic brain injury. J Neuroinflammation 17:89.

Maas AIR, Menon DK, Adelson PD, Andelic N, Bell MJ, Belli A, Bragge P, Brazinova A, Büki A, Chesnut RM, Citerio G, Coburn M, Cooper DJ, Crowder AT, Czeiter E, Czosnyka M, Diaz-Arrastia R, Dreier JP, Duhaime AC, Ercole A, et al. (2017) Traumatic brain injury: integrated approaches to improve prevention, clinical care, and research. Lancet Neurol 16:987-1048.

Malhotra S, Costa C, Eixarch H, Keller CW, Amman L, Martínez-Banaclocha H, Midaglia L, Sarró E, Machín-Díaz I, Villar LM, Triviño JC, Oliver-Martos B, Parladé LN, Calvo-Barreiro L, Matesanz F, Vandenbroeck K, Urcelay E, Martínez-Ginés ML, Tejeda-Velarde A, Fissolo N, et al. (2020) NLRP3 inflammasome as prognostic factor and therapeutic target in primary progressive multiple sclerosis patients. Brain 143:1414-1430.

Martin-Blondel G, Brassat D, Bauer J, Lassmann H, Liblau RS (2016) CCR5 blockade for neuroinflammatory diseases--beyond control of HIV. Nat Rev Neurol 12:95-105.

Miyamoto N, Magami S, Inaba T, Ueno Y, Hira K, Kijima C, Nakajima S, Yamashiro K, Urabe T, Hattori N (2020) The effects of A1/A2 astrocytes on oligodendrocyte linage cells against white matter injury under prolonged cerebral hypoperfusion. Glia 68:1910-1924.

Morganti-Kossmann M, Semple B, Hellewell S, Bye N, Ziebell J (2019) The complexity of neuroinflammation consequent to traumatic brain injury: from research evidence to potential treatments. Acta Neuropathol 137:731-755.

O'Brien W, Pham L, Symons G, Monif M, Shultz S, McDonald S (2020) The NLRP3 inflammasome in traumatic brain injury: potential as a biomarker and therapeutic target. J Neuroinflammation 17:104.

Paudel YN, Angelopoulou E, Piperi C, Othman I, Shaikh MF (2020) HMGB1-mediated neuroinflammatory responses in brain injuries: potential mechanisms and therapeutic opportunities. Int J Mol Sci 21:4609.

Peng AYT, Agrawal I, Ho WY, Yen YC, Pinter AJ, Liu J, Phua QXC, Koh KB, Chang JC, Sanford E, Man JHK, Wong P, Gutmann DH, Tucker-Kellogg G, Ling SC (2020). Loss of TDP-43 in astrocytes leads to motor deficits by triggering A1-like reactive phenotype and triglial dysfunction. Proc Natl Acad Sci U S A 117:29101-29112.

Rabinowitz AR, Levin HS (2014). Cognitive sequelae of traumatic brain injury. Psychiatr Clin North Am 37:1-11.

Ran H, Yuan J, Huang J, Wang J, Chen K, and Zhou Z (2020) Adenosine A(2A) Receptors in bone marrow-derived cells attenuate cognitive impairment in mice after chronic hypoperfusion white matter injury. Transl Stroke Res 11:1028-1040.

Ren H, Kong Y, Liu Z, Zang D, Yang X, Wood K, Li M, Liu Q (2018) Selective NLRP3 (pyrin domain-containing protein 3) inflammasome inhibitor reduces brain injury after intracerebral hemorrhage. Stroke 49:184-192.

Rosi S, Pert CB, Ruff MR, McGann-Gramling K, Wenk GL (2005) Chemokine receptor 5 antagonist D-Ala-peptide T-amide reduces microglia and astrocyte activation within the hippocampus in a neuroinflammatory rat model of Alzheimer's disease. Neuroscience 134:671-676.

Roth TL, Nayak D, Atanasijevic T, Koretsky AP, Latour LL, McGavern DB (2014) Transcranial amelioration of inflammation and cell death after brain injury. Nature 505:223-228.

Sacks D, Baxter B, Campbell BCV, Carpenter JS, Cognard C, Dippel D, Eesa M, Fischer U, Hausegger K, Hirsch JA, Shazam Hussain M, Jansen O, Jayaraman MV, Khalessi AA, Kluck BW, Lavine S, Meyers PM, Ramee S, Rüfenacht DA, Schirmer CM, et al. (2018) Multisociety consensus quality improvement revised consensus statement for endovascular therapy of acute ischemic stroke. Int J Stroke 13:612-632.

Schneider CA, Rasband WS, Eliceiri KW (2012) NIH Image to ImageJ: 25 years of image analysis. Nat Methods 9:671-675.

Silver J, Miller JH (2004) Regeneration beyond the glial scar. Nat Rev Neurosci 5:146-156.

Simon DW, McGeachy MJ, Bayır H, Clark RS, Loane DJ, Kochanek PM (2017) The far-reaching scope of neuroinflammation after traumatic brain injury. Nat Rev Neurol 13:171-191.

Skelly DT, Griffin É W, Murray CL, Harney S, O'Boyle C, Hennessy E, Dansereau MA, Nazmi A, Tortorelli L, Rawlins JN, Bannerman DM, Cunningham C (2019) Acute transient cognitive dysfunction and acute brain injury induced by systemic inflammation occur by dissociable IL-1-dependent mechanisms. Mol Psychiatry 24:1533-1548.

Sofroniew MV (2015) Astrocyte barriers to neurotoxic inflammation. Nat Rev Neurosci 16:249-263.

Sun Q, Wang S, Chen J, Cai H, Huang W, Zhang Y, Wang L, Xing Y (2019) MicroRNA-190 alleviates neuronal damage and inhibits neuroinflammation via Nlrp3 in MPTP-induced Parkinson's disease mouse model. J Cell Physiol 234:23379-23387.

Wang X, Deckert M, Xuan NT, Nishanth G, Just S, Waisman A, Naumann M, Schlüter D (2013) Astrocytic A20 ameliorates experimental autoimmune encephalomyelitis by inhibiting NF-κB- and STAT1-dependent chemokine production in astrocytes. Acta Neuropathol 126:711-724.

Witcher K, Eiferman D, Godbout J (2015) Priming the inflammatory pump of the CNS after traumatic brain injury. Trends Neurosci 38:609-620.

Wu X, Yang Z, Wang H, Zhao Y, Gao X, Zang B (2021) High-mobility group box protein-1 induces acute pancreatitis through activation of neutrophil extracellular trap and subsequent production of IL-1β. Life Sci 286:119231.

Xiong XY, Liu L, Yang QW (2016) Functions and mechanisms of microglia/macrophages in neuroinflammation and neurogenesis after stroke. Prog Neurobiol 142:23-44.

Xu GG, Guo J, Wu Y. Chemokine receptor CCR5 antagonist maraviroc: medicinal chemistry and clinical applications. Curr Top Med Chem. 2014;14(13):1504-14.

Xu X, Yin D, Ren H, Gao W, Li F, Sun D, Wu Y, Zhou S, Lyu L, Yang M, Xiong J, Han L, Jiang R, and Zhang J (2018a) Selective NLRP3 inflammasome inhibitor reduces neuroinflammation and improves long-term neurological outcomes in a murine model of traumatic brain injury. Neurobiol Dis 117:15-27.

Xu X, Zhang A, Zhu Y, He W, Di W, Fang Y, Shi X (2018b) MFG-E8 reverses microglial-induced neurotoxic astrocyte (A1) via NF-κB and PI3K-Akt pathways. J Cell Physiol 234:904-914.

Yan C, Yan H, Mao J, Liu Y, Xu L, Zhao H, Shen J, Cao Y, Gao Y, Li K, Jin W (2020) Neuroprotective effect of oridonin on traumatic brain injury via inhibiting NLRP3 inflammasome in experimental mice. Front Neurosci 14:557170.

Yang LY, Greig NH, Huang YN, Hsieh TH, Tweedie D, Yu QS, Hoffer BJ, Luo Y, Kao YC, Wang JY (2016) Post-traumatic administration of the p53 inactivator pifithrin-α oxygen analogue reduces hippocampal neuronal loss and improves cognitive deficits after experimental traumatic brain injury. Neurobiol Dis 96:216-226.

Yun SP, Kam TI, Panicker N, Kim S, Oh Y, Park JS, Kwon SH, Park YJ, Karuppagounder SS, Park H, Kim S, Oh N, Kim NA, Lee S, Brahmachari S, Mao X, Lee JH, Kumar M, An D, Kang SU, et al. (2018). Block of A1 astrocyte conversion by microglia is neuroprotective in models of Parkinson's disease. Nat Med 24:931-938.

Zamanian JL, Xu L, Foo LC, Nouri N, Zhou L, Giffard RG, Barres BA (2012) Genomic analysis of reactive astrogliosis. J Neurosci 32:6391-6410.

C-Editor: Zhao M; L-Editors: Li CH, Song LP, McRae M; T-Editor: Jia Y

Additional Table 1 Modified Neurological Severity Scoring (mNSS)

Motor tests	**6**
Raising mouse by tail	**3**
Flexion of forelimb	1
Flexion of hindlimb	1
Head moved >10° to vertical axis within 30s	1
Placing mouse on floor (normal=0; maximum=3)	**3**
Normal walk	0
Inability to walk straight	1
Circling toward paretic side	2
Falls down to paretic side	3
Sensory tests	**8**
Placing test (visual and tactile test)	**1**
Proprioceptive test (deep sensation, pushing paw against table edge to stimulate limb muscles)	**1**
Beam balance tests (normal=0; maximum=6)	**6**
Balances with steady posture	0
Grasps side of beam	1
Hugs beam and 1 limb falls down from beam	2
Hugs beam and 2 limb fall down from beam, or spins on beam (>60s)	3
Attempts to balance on beam but falls off (>40s)	4
Attempts to balance on beam but falls off (>20s)	5
Falls off; no attempt to balance or hang on to beam (<20s)	6
Reflex absence and abnormal movements	**4**
Pinna reflex (head shake when auditory meatus is touched)	1
Corneal reflex (eye blink when cornea is lightly touched with cotton)	1
Startle reflex (motor response to a brief noise from snapping a clipboard paper)	1
Seizures, myoclonus, myodystonia	1
Maximum points	**18**